Structural parameters determination of ALD-SnO_2 thin films grown on silicon (100) and boron-doped silicon (100) substrates

J. Rodríguez-López[a,*], R. Rangel[b], J. Lara-Romero[b], P. Quintana-Owen[c], P. Bartolo-Pérez[c], A. Ramos-Carrazco[d]
[a] *Valley Technological Institute of Morelia, National Technological Institute of México, Morelia, Michoacán, México*
[b] *Chemical Engineering Faculty, Michoacan University, Morelia, Michoacán, México. Morelia, Michoacán, México*
[c] *Applied Physics Deparment-CINVESTAV. Mérida, Yucatán, México*
[d] *Department of Physics Research, University of Sonora. Hermosillo, Sonora, México.*

The present study describes the synthesis of SnO_2 thin films achieved by the atomic layer deposition technique based on the reaction of tetrakis(dimethylamino)tin ($Sn(NMe_2)_4$ and H_2O. The experiments were realized at 2.7×10^{-4} atm and 150 °C on silicon, or boron-doped silicon substrates. To characterize the physicochemical properties of the films, XRD was used to calculate the structural parameters of SnO_2 thin films. Also, SEM, XPS, Raman, and UV-Vis spectroscopy techniques were used to understand the morphology, composition, and optical properties. The results indicate that the procedure presented here offers a viable alternative for fabricating high-quality SnO2 thin films that can be used in various technological fields, such as sensors, electronic, and optoelectronic devices.

(Received June 21, 2024; Accepted September 13, 2024)

Keywords: Semiconductor, SnO_2, Atomic layer deposition, Thin films

1. Introduction

SnO_2 is a material with a band gap energy of 3.6 eV at 300 K, and an excitation binding energy of 130 mV at 293 K. It has attracted attention towards many applications such as gas sensors, lithium-ion batteries, photovoltaic electrodes, laser, detectors, devices optoelectronics, antimicrobial, photocatalysts, etc. [1–7] Currently, the control of size, morphology, and crystalline structure of the materials have become key factors for obtaining multifunctional materials with new properties and various technological applications, directly related to the synthesis method. In parallel with the large number of applications, nowadays, there are various techniques for the synthesis of SnO2 thin films such as metal-organic chemical vapor deposition (MOCVD), chemical spray pyrolysis, thermal evaporation, and atomic layer deposition (ALD), to mention a few [8–11]. Among them, ALD is a technique based on sequential and self-limited reactions on the surface of a substrate, which generate a film through each deposition cycle [12]. The main advantages provided by the technique are the control of the chemical composition and thickness of the film. Besides, it can be used on substrates with complex shapes, resulting in films with a low number of defects and high quality [13]. As occurs in many processes, the choice of precursors is a key point in carrying out a successful synthesis, prioritizing the use of easy-to-handle and environmentally friendly compounds. In the present study, tetrakis(dimethylamino)tin was suggested as a precursor of Sn due to the recent importance it has acquired in the fabrication of SnO_2 thin films because it can react with various reagents such as water, ozone, and butanol, at relatively low deposition temperatures (<250 ◦ C), another advantage is that no by-products are produced that damage the deposit system [11,14–16]. Besides, we investigate the possible effect of the type of substrate and the synthesis conditions on the physicochemical properties of SnO_2 thin films prepared by ALD, for its potential use in sensors, electronic and optoelectronic devices, among others.

* Corresponding author: jrl_ibqa@hotmail.com
https://doi.org/10.15251/JOR.2024.205.627

2. Experimental

SnO_2 thin films were deposited by Savanah 100 ALD equipment, using silicon (100) N-type without dopants, and boron-doped silicon (100) P-type as substrates. The substrates were cleaned with H_2SO_4, HF, HCl, and deionized water, respectively. Before introducing the substrates into the ALD system, they were dried at room temperature with a nitrogen gas flow. Tetrakis(dimethylamino)tin ($Sn(NMe_2)_4$) and deionized water were used as precursors; while N_2 (99.999%) was used as a carrier and purge gas. The pulse and purge time were kept constant at 0.5/30/0.015/30 s for $Sn(NMe_2)_4/N_2/H_2O/N_2$, respectively. After 1050 deposit cycles, with a growth rate of 0.064 nm/cycle, thin films were obtained with a thickness of about 68 nm, in accordance with the rate growth shown in Fig. 1a. Finally, the films were calcined at 400 °C for 4 h to obtain the tetragonal crystal structure of SnO_2. The synthesized films were designated as STO (silicon) and BSTO (boron-doped silicon), according to the used substrate.

XRD analyses were performed on a Siemens-D 500 diffractometer with monochromatic radiation of CuKα = 1.54 Å, at 25 mA and 34 keV. Morphological studies were obtained using a field emission scanning electron microscope (FESEM, JSM-7600F JEOL. The XPS studies were acquired with a Thermo Scientific K-Alpha equipment equipped with an AlKα monochromator. Raman spectra were acquired using a WItec alpha 300 Raman spectrometer employing a 633 nm laser. UV-Vis spectroscopy determinations were performed using an AvaSpec-2048 spectrometer under reflection mode. A Horiba Ellipsometer was used to determine the film thickness.

3. Results and discussion

Fig. 1b shows the diffraction patterns for SnO_2 thin films. In those analyses, the characteristic peaks allocated to the tetragonal structure of SnO_2 were detected, in accordance with ICCD 41-1445 diffraction data card. The structural parameters such as crystallite size (D), texture coefficient (T_c), lattice parameters, $a = b$ and c, unit cell volume (V), dislocation density (ρ), micro-strain (ε), and stacking fault (SF) for SnO_2 thin films were determined using the XRD patterns and the corresponding formulas described in the references [5,10,17,18] shown below, the calculated data are reported in Table 1. The STO film shows preferential growth along the (101) plane; while the BSTO film grows preferentially along the (110) plane, which may indicate that the substrate influences the deposit process and generate changes in the growth orientation of the films. The crystallite size obtained by means of the Scherrer equation for the STO and BSTO films is 8.97 and 10.36 nm, respectively. Table 1 shows that the lattice parameters of the SnO_2 films agree with the values reported for the tetragonal structure of SnO_2 ($a = b$ = 4.738 Å and c = 3.187 Å, ICCD 41-1445). Furthermore, the low values of ρ, ε, and SF can be attributed to a low number of defects, suggesting that SnO_2 compounds are high-quality thin films.

$$D = \frac{0.9\lambda}{B\cos\theta} \tag{1}$$

$$T_{c(hkl)} = \frac{I_{(hkl)}/I_{r(hkl)}}{\left[\frac{1}{n}\sum\left(\frac{I_{(hkl)}}{I_{r(hkl)}}\right)\right]} \tag{2}$$

$$d_{2(hkl)} = \sin\theta = m\lambda \tag{3}$$

$$\frac{1}{d^2} = \frac{h^2+k^2}{a^2} + \frac{l^2}{c^2} \tag{4}$$

$$V = a^2c \tag{5}$$

$$\rho = \frac{1}{D^2} \tag{6}$$

$$\varepsilon = \frac{(\beta\, cos\theta)}{4} \quad (7)$$

$$SF = \frac{2\pi^2}{45(3tan\theta)^{1/2}} \quad (8)$$

Table 1. Calculated structural parameters of SnO_2 thin films.

Sample	Crystal plane	T_c	D(nm)	a = b (Å)	c (Å)	V (Å^3)	ρ (cm^{-2})	ε (× 10^{-3})	SF
STO	(101)	1.55	8.97	4.7317	3.1420	70.30	0.0124	4.51	0.1452
BSTO	(110)	1.42	10.36	4.7178	3.2173	71.61	0.0093	3.57	0.1655

In Fig. 1c, the observed morphology in STO film consists of spherical nanocrystals whose sizes range from 30 to 100 nm, with a homogeneous coating on the surface´s substrate. Fig. 1d shows an even coating of the surface, ranging from 10 to 30 nm, shaped as small aggregates which resemble spheres, whose diameter range from 80 to 100 nm.

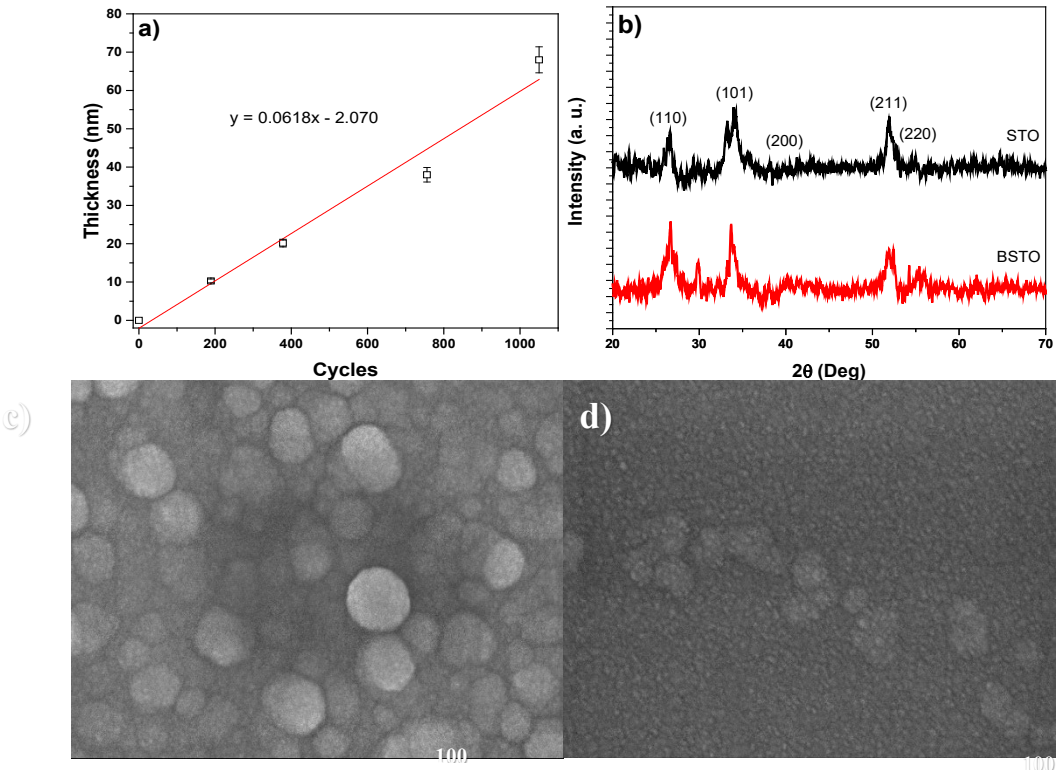

Fig. 1. a) GPC of SnO_2 produced by ALD technique, b) XRD of SnO_2 thin films, c) FE-SEM micrograph of STO film and d) FE-SEM micrograph of BSTO film.

Fig. 2a displays the XPS survey spectra for the SnO_2 thin films calibrated using the C1s peak situated at 284.78 eV as a reference. The respective peaks for tin and oxygen elements were found. The high-resolution (H-R) scan for Sn3d is displayed in Fig. 2b. The binding energy signals located at 486.48 and 494.98 eV are attributed to the spin-orbit $Sn3d_{5/2}$ and $Sn3d_{3/2}$, respectively [8,10]. Also, H-R scanning for O1 reveals the presence of two signals (Fig. 2c). The signal with low binding energy, placed at 530.39 eV is related to O^{2-} ions in the SnO_2 structure (O-Sn^{4+} bonds) [19]; while the high-energy signal is related to chemisorbed oxygen species and hydroxyl ions [20]. No

signal was detected at 100 eV which is associated with Si2p, thus confirming the homogeneous deposit of SnO_2 on the surface of both substrates.

Fig. 2d shows the Raman spectra of the SnO_2 films. The peaks at 303 cm^{-1}, 520 cm^{-1}, and 620 cm^{-1} correspond to the silicon used as substrate [21]. For the SnO_2 films the mode A_{1g} at 639 cm^{-1}, was located, which is associated with vibrational modes of Sn-O bonds along the plane perpendicular to the *c-axis* [22]; on the other hand, the E_g mode found at 474 cm^{-1} is associated to the oxygen vibration on the *c-axis* direction. This signal is highly sensitive to oxygen vacancies [20]. On the other hand, the A_{2u} (LO) mode was detected at 673 cm^{-1} [23]. Confirming the tetrahedral coordination of SnO_2.

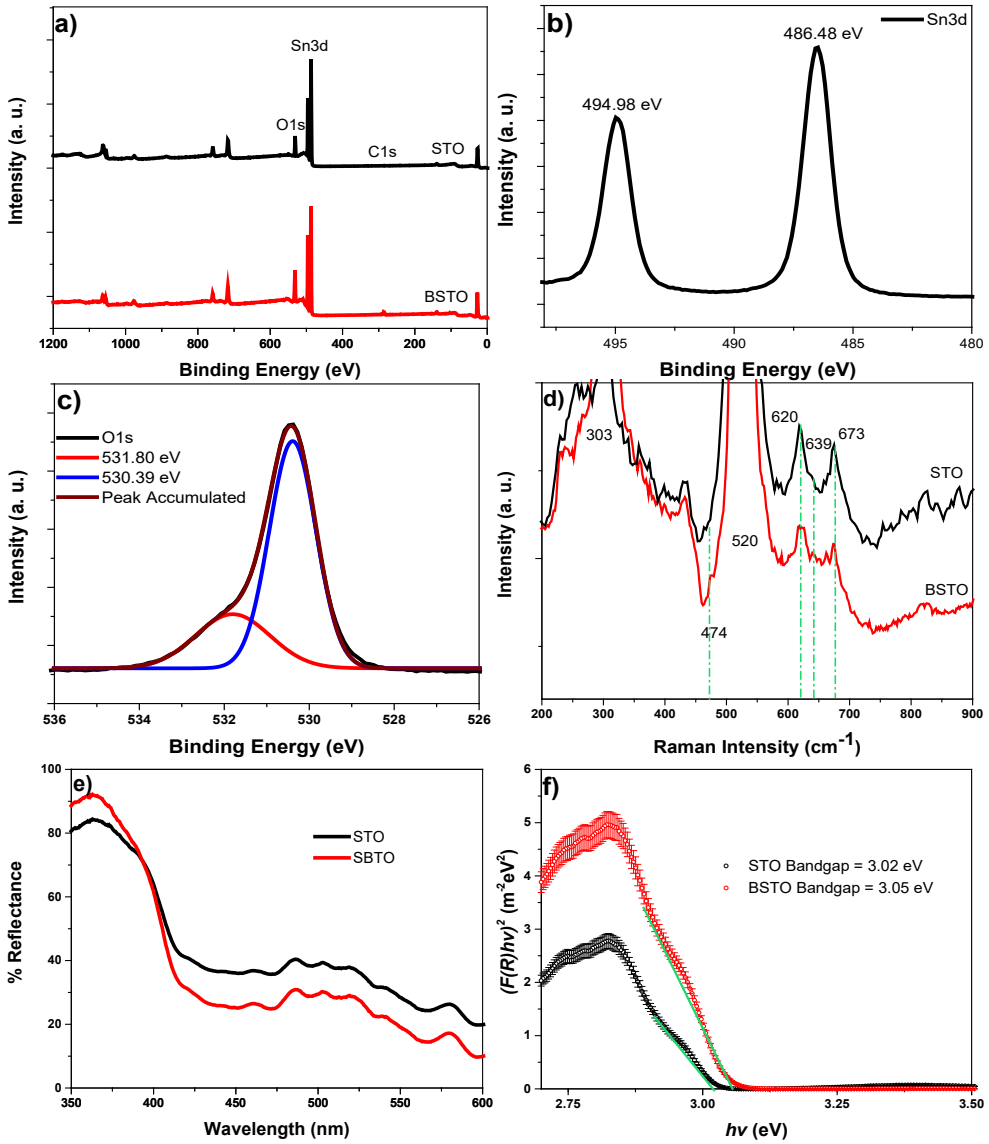

Fig. 2. a) General survey XPS spectra of SnO_2 thin films, b) H-R scan of Sn3d for STO, c) H-R scan of O1s for BSTO. d) Raman spectra of SnO_2 thin films. e) Diffuse reflectance of SnO_2 thin films. f) Absorption edge spectra of SnO_2 thin flims using Kubelka–Munk approach.

The diffuse reflectance spectra (DRS) of the SnO_2 thin films are shown in Fig. 2e. The reflectance spectra were converted into absorption spectra using the Kubelka-Munk and Tauc approach, according to the reference [24].

$$F(R) = \frac{(1-R)^2}{2R} \quad (9)$$

$$(F(R)hv)^2 \propto (hv - E_g) \quad (10)$$

The band gap energy (E_g) of the films was determined from the $F(R)hv^2$ vs hv (Fig. 2f) graph, extrapolating the linear contribution of the graph against the axis of the excitation energy $F(R)hv^2 = 0$. The calculated E_g values are 3.02 eV and 3.05 eV, for STO and BSTO films, respectively; these values are lower than those reported in the literature for SnO_2 films [9]. This reduction in their E_g can be attributed to the synthesis method, which could create high-density point defects (oxygen vacancies), which allowed reducing the E_g of the SnO_2 films [25].

The results confirm that the ALD technique is an efficient method for the synthesis of high-quality SnO_2 thin films. Besides, the influence of the substrate is observed, for instance, B-doped silicon produces a film with fewer defects and a larger crystallite size; while silicon favors a more defined morphology, as well as a lower energy value in its E_g. In addition, the materials manufactured in this work can open a way to control specific properties in thin films, favoring the generation of nanomaterials with a wide room potential application in various technological areas.

4. Conclusions

The results show that the proposed experimental operating conditions allowed the successful synthesis of SnO_2 thin films through an ALD deposit process. The tetragonal structure of SnO_2 was confirmed by XRD analysis, and the films showed a crystallite size of approximately 10 nm. The fabricated films have a low defect density. Optical properties of the films show an energy absorption in the visible region. Besides, the substrate appears to be a critical factor affecting the preferential growth, morphology and light absorption of the films, where the STO film showed the lowest Eg (3.02 eV). These results demonstrate that SnO_2 thin films can be viable materials for application in different technological fields, as well as for use as templates for further growth of nanostructured materials.

Acknowledgments

J. Rodríguez-López acknowledges scholarship provided by CONACYT-México. R. Rangel acknowledges CIC-UMSNH-2024 project. Authors thank to CINVESTAV-IPN, Unidad Mérida. To W. Cauich, D. Aguilar, J. Bante, and D. Macías for their technical support. Also, thank LANBIO-CINVESTAV and FOMIX-Yucatán 2008-108160 Conacyt LAB-2009-01-123913, 292692, 294643 projects.

References

[1] R. G. Pavelko, M. Yuasa, T. Kida, K. Shimanoe, N. Yamazoe, Sensors Actuators, B Chem. 210, 719 (2015); https://doi.org/10.1016/j.snb.2015.01.038

[2] D. Narsimulu, S. Vinoth, E. S. Srinadhu, N. Satyanarayana, Ceram. Int. 44, 201 (2018); https://doi.org/10.1016/j.ceramint.2017.09.159

[3] A. Martyła, Ł. Majchrzycki, P. Marciniak, B. Sztorch, M. Kopczyk, R. Przekop, Chemik 67, 1207 (2013).

[4] J. Pan, H. Shen, S. Mathur, J. Nanotechnol. (2012); https://doi.org/10.1155/2012/917320

[5] K. Sujatha, T. Seethalakshmi, A. P. Sudha, O. L. Shanmugasundaram, Nano-Structures and Nano-Objects 18, 100305 (2019); https://doi.org/10.1016/j.nanoso.2019.100305

[6] X. Chen, D. Chu, L. Wang, W. Hu, H. Yang, J. Sun, S. Zhu, G. Wang, J. Tao, S. Zhang, J. Alloys Compd. 729, 710 (2017); https://doi.org/10.1016/j.jallcom.2017.08.094

[7] S. Suthakaran, S. Dhanapandian, N. Krishnakumar, N. Ponpandian, J. Mater. Sci. Mater. Electron. 30, 13174 (2019); https://doi.org/10.1007/s10854-019-01681-7

[8] S. Y. Turishchev, O. A. Chuvenkova, E. V. Parinova, D. A. Koyuda, R. G. Chumakov, M. Presselt, A. Schleusener, V. Sivakov, Results Phys. 11, 507 (2018); https://doi.org/10.1016/j.rinp.2018.09.046

[9] R. Lotfi Orimi, M. Maghouli, Optik (Stuttg). 127, 263 (2016); https://doi.org/10.1016/j.ijleo.2015.10.033

[10] S. M. Ingole, Y. H. Navale, D. K. Bandgar, V. B. Patil, S. T. Navale, F. J. Stadler, N. S. Ramgir, S. K. Gupta, D. K. Aswal, R. S. Mane, J. Colloid Interface Sci. 493, 162 (2017); https://doi.org/10.1016/j.jcis.2017.01.025

[11] J. H. Bang, N. Lee, A. Mirzaei, M. S. Choi, H. G. Na, C. Jin, W. Oum, S. Shin, H. S. Choi, H. Park, Y. Choi, H. Jeon, H. W. Kim, Ceram. Int. 45, 7723 (2019); https://doi.org/10.1016/j.ceramint.2019.01.074

[12] T. Muneshwar, M. Miao, E. R. Borujeny, K. Cadien, in Handb. Thin Film Depos. (Elsevier, 2018), pp. 359-377; https://doi.org/10.1016/B978-0-12-812311-9.00011-6

[13] I. Levchuk, C. Guillard, F. Dappozze, S. Parola, D. Leonard, M. Sillanpää, Journal Photochem. Photobiol. A Chem. 328, 16 (2016); https://doi.org/10.1016/j.jphotochem.2016.03.034

[14] U. Farva, J. Kim, Mater. Chem. Phys. 267, 124584 (2021); https://doi.org/10.1016/j.matchemphys.2021.124584

[15] D. won Choi, J. S. Park, Surf. Coatings Technol. 259, 238 (2014); https://doi.org/10.1016/j.surfcoat.2014.02.012

[16] E. C. Nwanna, P. E. Imoisili, T. C. Jen, J. King Saud Univ. - Sci. 34, 102123 (2022); https://doi.org/10.1016/j.jksus.2022.102123

[17] S. Ben Ameur, H. Bel hadjltaief, A. Barhoumi, B. Duponchel, G. Leroy, M. Amlouk, H. Guermazi, Vacuum 155, 546 (2018); https://doi.org/10.1016/j.vacuum.2018.05.051

[18] T. Prasada Rao, M. C. Santhoshkumar, Appl. Surf. Sci. 255, 7212 (2009); https://doi.org/10.1016/j.apsusc.2009.03.065

[19] V. Aravindan, K. B. Jinesh, R. R. Prabhakar, V. S. Kale, S. Madhavi, Nano Energy 2, 720 (2013); https://doi.org/10.1016/j.nanoen.2012.12.007

[20] S. Deepa, K. Prasanna Kumari, B. Thomas, Ceram. Int. 43, 17128 (2017); https://doi.org/10.1016/j.ceramint.2017.09.134

[21] Y. Zhang, B. Lin, Z. Fu, C. Liu, W. Han, Opt. Mater. (Amst). 28, 1192 (2006); https://doi.org/10.1016/j.optmat.2005.08.016

[22] A. R. Kamali, D. J. Fray, Mater. Sci. Eng. B Solid-State Mater. Adv. Technol. 177, 819 (2012); https://doi.org/10.1016/j.mseb.2012.03.035

[23] D. Zhao, X. Wu, Mater. Lett. 210, 354 (2018); https://doi.org/10.1016/j.matlet.2017.09.068

[24] K. Ocakoglu, S. A. Mansour, S. Yildirimcan, A. A. Al-Ghamdi, F. El-Tantawy, F. Yakuphanoglu, Spectrochim. Acta - Part A Mol. Biomol. Spectrosc. 148, 362 (2015); https://doi.org/10.1016/j.saa.2015.03.106

[25] F. Fang, Y. Zhang, X. Wu, Q. Shao, Z. Xie, Mater. Res. Bull. 68, 240 (2015); https://doi.org/10.1016/j.materresbull.2015.03.072